emitted, then we must conclude that with increasing excitation energy neutron emission increases faster for the heavy fragment than it does for the light fragment. This supports the evidence presented by McHugh,[8] who concluded that $d\nu/dE$ was greater for the heavy fragment than for the light. Therefore, the assumption that $\nu_L=\nu_H$ throughout the energy range cannot hold. The method of calculating independent fission yields at different excitation energies proposed by Coryell *et al.*[6] is based in part on the assumption that $\nu_L=\nu_H$ and particularly implies that $d\nu_L/dE=d\nu_H/dE$. Hence it appears to be in error in this respect. On the basis of what limited evidence we have, it appears reasonable to use a value of $\sim$0.047 for dZ_p/dE for heavy fragments, and a value of $\sim$0.023 for light fragments. However, one must exercise caution in extrapolating to or from thermal-neutron fission, especially for nuclides near closed shells.

We would like to point out that the difference in dZ_p/dE for the light and heavy fragments has some implications concerning the use of the equal charge displacement (ECD) rule. As is well known, most of the data for thermal-neutron fission are in agreement with a single charge dispersion curve, with Z_p values calculated from the empirical ECD rule. The fact that the Z_p value for a heavy fragment may change with energy faster than that for a light fragment implies that the ECD rule will be increasingly less successful in correlating data for different mass numbers as the excitation energy is raised.

(3) The inescapable conclusion is that the prediction of independent fission yields at different excitation energies is still fraught with danger. We would like to point out the need for independent yield data from fission with excitation energies of 8 to 18 MeV. The large gap that exists here makes the interpolation from thermal-neutron fission data to higher energy data difficult, and may be hiding important details resulting from shell effects. Unfortunately, experimental data in this area are very difficult to obtain.

PHYSICAL REVIEW VOLUME 139, NUMBER 6B 20 SEPTEMBER 1965

Cross Sections for the Production of Li^9, C^{16}, and N^{17} in Irradiations with GeV-Energy Protons*

I. DOSTROVSKY,† R. DAVIS, JR., A. M. POSKANZER, AND P. L. REEDER
Chemistry Department, Brookhaven National Laboratory, Upton, New York
(Received 8 April 1965)

Twenty-five targets ranging from boron to uranium were irradiated with 1.0- and 2.8-GeV-energy protons. Cross sections for the production of the nuclides Li^9, C^{16}, and N^{17} were measured by counting the delayed neutrons which they emit. No longer lived delayed-neutron emitters were observed except those produced as fission products from uranium. Cross sections for the latter are presented and interpreted in terms of low-deposition-energy processes. Cross sections for the nuclides Li^9, C^{16}, and N^{17} from the lightest targets are interpreted as simple spallation products, mainly from (p,xp) reactions. Several pairs of targets with similar mass number and differing neutron-to-proton ratio were studied. A strong dependence of the cross sections on the neutron-to-proton ratio of the target was observed, especially for the lighter mass regions. Relative cross-section calculations were performed for the heavier targets assuming these and other light fragments were evaporated from excited knock-on cascade products. The effect of secondary evaporation from excited evaporated fragments was included. The experimental and calculated relative cross sections agree well with respect to their dependence on the mass number and neutron-to-proton ratios of the target. It is concluded that the mass-energy surface, which is included in the evaporation formalism, is important in determining the relative yields of light fragments.

INTRODUCTION

THE formation of light fragments (mass 6–24) in considerable yields is one of the characteristics of the interaction of high-energy particles with complex nuclei. Previous investigations of these reactions included measurements of the cross section for the formation of He^6,[1] Be^7,[2] Li^8,[3] C^{11},[4] N^{13},[5] F^{18},[6] and Na^{24} [6] from a range of target nuclei bombarded with GeV-

* Research performed under the auspices of the U. S. Atomic Energy Commission.
† On leave of absence from the Weizmann Institute of Science, Rehovoth, Israel.

[1] F. S. Rowland and R. L. Wolfgang, Phys. Rev. **110**, 175 (1958).
[2] E. Baker, G. Friedlander, and J. Hudis, Phys. Rev. **112**, 1319 (1958); J. Hudis, 1964 (private communication).
[3] S. Katcoff, Phys. Rev. **114**, 905 (1959).
[4] R. Sharp (private communication).
[5] I. Dostrovsky, Z. Fraenkel, and J. Hudis, Phys. Rev. **123**, 1452 (1961).
[6] A. A. Caretto, Jr., J. Hudis, and G. Friedlander, Phys. Rev. **110**, 1130 (1958).

energy protons. Also the spallation of aluminum has been studied.[7] The variation of the cross section with the mass number A of the target nucleus seems to depend on the particular product examined. Thus, while Be^7 shows little if any dependence on the mass of the target, the He^6 cross section increases with A, and N^{13} decreases with A. Some products (F^{18}, Na^{24}) show a double branched curve, the cross section decreasing to a minimum at a certain value of A of the target and then rising again. The behavior of the cross sections of light fragments as a function of target mass suggest that more than one mechanism is operating in their production by high-energy reactions.[6]

The present experiments were undertaken with a view to shedding further light on the problem of light-fragment emission. In particular we tried to establish in greater detail the dependence of the cross section on the mass of the target, and to increase the range of products measured so far by investigating isotopes further from beta stability. We chose for study the delayed-neutron emitters Li^9, C^{16}, and N^{17}. Delayed neutron emission is sufficiently rare to provide a distinctive "signature" by which these isotopes can be unambiguously measured even in the presence of a large number of other activities. In addition the half-lives of these isotopes are sufficiently different that the contributions of each could be resolved. Because of this it became possible to measure the formation cross sections of these products under strictly comparable conditions from a wide range of targets. The properties of the isotopes are presented in Table I.

TABLE I. Properties of Li^9, C^{16}, and N^{17}.

Nuclide	Half-life (sec)	Total neutron branch (%)	Neutron energy (MeV)
Li^9	0.176±0.001[a]	75±15[b]	0.7(≈92%), 3–4.5(≈8%)[b]
C^{16}	0.74 ±0.03[c]	?	?
N^{17}	4.16 ±0.01[a]	95±1[d]	0.40(47%), 1.22(47%), 1.79(6%)[e]

[a] This work.
[b] D. E. Alburger, Phys. Rev. **132**, 328 (1963).
[c] S. Hinds, R. Middleton, A. E. Litherland, and D. J. Pullen, Phys. Rev. Letters **6**, 113 (1961).
[d] M. G. Silbert and J. C. Hopkins, Phys. Rev. **134**, B16 (1964).
[e] J. Gilat, G. D. O'Kelley, and G. Eichler, Bull. Am. Phys. Soc. **8**, 320 (1963); Oak Ridge National Laboratory Report, ORNL-3488, 1963 (unpublished).

EXPERIMENTAL

The targets were irradiated in the external beam of the Brookhaven Cosmotron at proton energies of 1.0 and 2.8 GeV. The Cosmotron is a pulsed accelerator with a normal beam intensity of about 10^{11} protons per pulse in the location of our experiment. The length of the beam pulse was about 1 msec and the machine repetition time about 4 sec. The target, after the irradiation pulse, was transported by means of a pneumatically operated mechanism into a high-efficiency neutron counter and the decay of the induced neutron activity was recorded by a 400-channel multiscaler. The general arrangement is shown in Fig. 1.

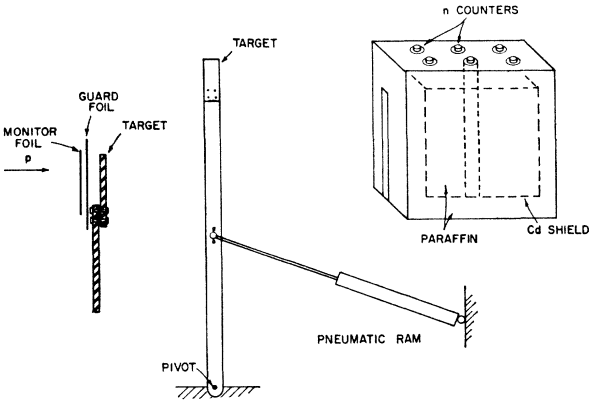

FIG. 1. General arrangement of apparatus for delayed-neutron counting.

The neutron detector consisted of a block of paraffin wax 38×41×63 cm in which were imbedded six $B^{10}F_3$ proportional counters, each 4.1 cm in diameter and 61 cm long. The outputs from the six counters were paralleled, and the signals, after suitable amplification and discrimination, were sent to the 400-channel multiscaler. The paraffin block was encased in a cadmium box and shielded by a 5-cm layer of paraffin. The whole counter assembly was contained in a sheet-metal box. A slot was provided through which the irradiated targets were introduced in the center of the detector. The efficiency of the detector for neutrons from a calibrated Ra–Be source (obtained from the Radiochemical Center, Amersham, England) was 9.25%. Periodic checks of the counting efficiency were carried out throughout the measurements. The efficiency of the counter for neutrons originating in the target irradiation position, which was about 1 m away, was 62 times lower. The sensitivity of the counter to Co^{60} γ rays was found to be negligible. The importance of the contribution of photoneutrons produced from the natural deuterium content of the paraffin by high-energy γ rays from the target was determined by observing the counting rate with an extra 200 g of D_2O placed at the center of the counter. No effect was observed. It was also noted that there was no difference in the neutron activities from D_2O and H_2O targets.

In separate experiments the dependence of the detector efficiency on neutron energy was measured. For this purpose neutron sources were prepared from Na^{24}-Be (0.83-MeV n), Na^{24}-D_2O (0.27 MeV), Sb^{124}-Be (0.024 MeV), and Pu-Be (3.9 MeV average n energy). These sources were standardized against the Ra-Be source using a Hansen long counter and the reported

[7] J. B. Cumming, J. Hudis, A. M. Poskanzer, and S. Kaufman, Phys. Rev. **128**, 2392 (1962).

TABLE II. Targets.

Target element	Chemical form	Physical form	Mechanical form[a]	Thickness (g/cm²)	Comments
Li	element	metal	cell C	0.670	
Be	element	metal	plate	0.651	
B	element	powder	cell B	0.520	
C	$(CH_2)_n$	polyethylene	plate	0.355	86% C
O^{16}	water	liquid	cell D	0.589	
O^{18}	water	liquid	cell D	0.656; 0.619	97% D_2O^{18}
F	$(CF_2)_n$	Teflon	plate	0.132; 0.548; 0.783	76% F
Na	element	metal	cell C	1.257	
Mg	element	metal	plate	1.171	
Al	element	metal	plate	0.856	
Si	element	powder	cell B	0.955	
S	element	cast solid	cell B	1.471	
Ca	element	metal	plate	1.035	
Ti	element	metal	plate	1.448	
Ni	element	metal	plate	0.456	
Cu	element	metal	plate	1.331	
Nb	element	metal	plate	1.277	
Ag	element	metal	plate	0.538	
La	oxide	powder	cell B	0.820	81±2% La
Pr	oxide	powder	cell B	0.826	79±2% Pr
Nd	oxide	powder	cell B	0.653	73.5±2% Nd
Ta	element	metal	plate	0.902	
W	element	metal	plate	1.535	
Pb	element	metal	cell A	0.848	
U	element	metal	cell A	0.138; 0.55	

[a] Cell A—½ in. thick, 2 in. ×2 in. foil sandwiched between two 1-mil Ti windows. Cell B—½ in. thick, 2 in. ×2 in., two 1-mil Ti windows. Cell C—½ in. thick, 2 in. ×2 in., two 1-mil Ti windows. Cell D—½ in. thick, 2 in. diam, two 1-mil Ti windows.

efficiency curves.[8] The various neutron sources were then counted in our neutron detector and the efficiency for each neutron energy determined (see Fig. 2). From this and from the known abundance of the various neutron groups of Li^9 and N^{17} (see Table I) we calculated the efficiency of the detector for these isotopes. Relative to the efficiency for a Ra-Be source, these were 1.17 for Li^9, and 1.11 for N^{17}. Since no information is available regarding the energies of neutrons from C^{16} we have arbitrarily assumed the relative efficiency for counting these neutrons to be 1.11. Because the efficiency of our counter does not vary much with neutron energy it is thought that no great error is introduced by this assumption.

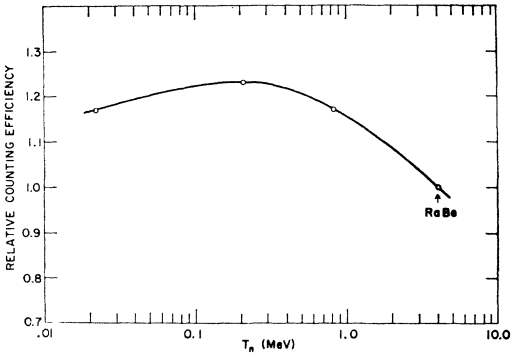

FIG. 2. Counting efficiency of the neutron counter versus neutron energy.

[8] J. De Pangher, Hanford Laboratory Report No. HW 56199, 1958 (unpublished).

The proton beam was focused to a spot about 1.5 cm in diameter. The targets, which were usually 5×5 cm in area intercepted almost the whole of the beam. Extensions were provided to all targets to permit their attachments to the pneumatically operated transport mechanism.

The target elements used in this research and their physical and chemical form are listed in Table II. Whenever possible the targets were made of sheets or thin plates of the element. Powders (boron and some oxides) and soft metals (Li, Na) were made into targets by pressing them into special aluminum frames fitted with two 0.025-mm titanium windows. Water targets (H_2O^{16}, D_2O^{16}, and D_2O^{18}) were in the form of circular aluminum cells 50 mm in diameter and 10 mm thick provided with 0.025-mm titanium windows. The transport of the target between the irradiation position in the beam and the neutron counter required about 200 msec. The target was moved to the count position after each proton pulse and was returned to the beam position just before the next pulse was due. The interval between beam pulses could be varied in multiples of the machine repetition time. The most commonly used multiples were one and six. With a repetition time of 4 sec these intervals gave a counting period of about 3 sec (10 msec/channel of the multiscaler) and 23 sec (100 msec/channel), respectively. These intervals were chosen so as to optimize the detection of both short-lived (176-msec Li^9) and longer lived (4.16-sec N^{17}) activities. In some of the experiments in which long-lived delayed neutrons were studied, counting periods of up to 2 min

(1 sec/channel) were used after irradiations by many beam pulses.

The whole cycle of target bombardment and neutron counting was repeated until sufficient neutron counts were accumulated for accurate decay-curve analysis. The equipment was controlled by an electronic programmer, synchronized with the Cosmotron and accurate to 1 msec which initiated each cycle. This programmer activated the pneumatic system of the target transport mechanism, enabled a proton beam to be accelerated, triggered the multiscaler on and off and in addition recorded elapsed time, the number of measurement cycles, total number of protons in the external beam, and the total number of neutrons detected. Although both pulse-by-pulse beam monitoring and integrated beam-intensity measurements were available from an ion chamber[9] 1 m upstream from the target, these did not seem to be sufficiently accurate for our purpose. The total number of protons traversing the target was obtained from a 0.025-mm Al monitor foil which was mounted about 2 cm upstream from the target. A guard foil of similar thickness was placed between the monitor foil and target to protect the former from Na^{24} atoms recoiling from the latter (see Fig. 1). After bombardment a piece of the monitor corresponding exactly in size with that of the target was cut out and after suitable delay (to allow F^{18} to decay) the Na^{24} activity induced in it was assayed with an end-window β counter. Corrections were applied for counting efficiency and for recoil loss.[10] A correction for the effect of the secondary particles from the targets on the monitor foil was made by lowering the monitor activity by $2\frac{1}{2}\%$ per g/cm^2 of target thickness. This number was determined from experiments with copper targets 2.8 and 14.2 g/cm^2 thick. The monitor cross sections used for the formation of Na^{24} from Al were 9.1 mb at 2.8 GeV and 10.5 mb at 1.0 GeV.[11]

The accumulated neutron counts in the multiscaler were printed out and, in the later experiments, punched out on paper tape. The data were then submitted to a computer and the decay curve analyzed.[12] The dead time of the counting system was 4 μsec. This was determined both by means of a double pulser and by fitting one of the decay curves which had the highest dead-time correction (30%). For all targets except uranium it was found that the decay curves resolved well with three components. The literature values[13] for the N^{17} and Li^9 half-lives are 4.14 ± 0.04 and 0.169 ± 0.003 sec, respectively. However, least-squares fits to our data gave values of 4.16 ± 0.01 and 0.176 ± 0.001 sec. These half-lives are listed in Table I and were used to analyze the data.[14] The activities of the three components when extrapolated to the time of the beam pulse were usually determined with a standard deviation of 1% for Li^9, 5% for C^{16}, and 1% for N^{17}. Whenever necessary, corrections were made for incomplete decay of the isotopes between irradiation pulses.

Background activity induced in air and the apparatus was found to be less than 1% for most self-supporting metal targets. It was determined under standard conditions but with no target attached to the pneumatic mechanism. For the powder and liquid targets blanks were determined by measuring the neutron activities induced in the empty powder holder or in the empty liquid cell. These blank corrections, arising out of activities induced in the aluminum frames and titanium windows, ranged up to a maximum of 35% (for rare-earth targets at 1 GeV). In all cases the neutron decay curves obtained in the background measurements were analyzed in terms of the half-lives of Li^9, C^{16}, and N^{17} and the initial activities of each component, after proper normalization for the intensity of bombardment, were subtracted from the corresponding gross activities observed for the target. The initial activities of the Teflon and oxide targets were further corrected for the contributions from carbon and oxygen using the measured cross section. The disintegration rates of Li^9 and N^{17} were calculated from the corrected initial activities and the known branching ratio for neutron emission of these isotopes (see Table I). A lower limit for the disintegration rate of C^{16} was obtained by assuming that all the decays proceed through neutron emission. While, therefore, we cannot at present obtain an absolute value for the C^{16} cross section, the comparison of the relative yields of this isotope obtained from various targets is valid.

The importance of secondary reactions was estimated by measuring the production of Li^9 and N^{17} from several thicknesses of Teflon (see Table II). Teflon was chosen for this purpose because it was considered that the simple reactions would be most sensitive to secondaries. An effect less than 3%/g/cm^2 was observed and therefore no secondary corrections were applied to any of the cross sections. Recoil loss from the targets has also been neglected. The Pb and U targets were sandwiched between two pieces of 0.025-mm Ti, making the effect minimal. It is estimated that the greatest recoil losses (2–4%) would occur for Li^9 from the Ni, Ag, and Ta targets. The results are presented in Table III. Most of the cross sections are the average of two or more determinations. From the agreement of duplicates it was de-

[9] C. E. Swartz, G. G. Levine, and R. L. Carmen, Rev. Sci. Instr. **34**, 1398 (1963).

[10] A. M. Poskanzer, J. B. Cumming, and R. Wolfgang, Phys. Rev. **129**, 374 (1963).

[11] J. B. Cumming, Ann. Rev. Nucl. Sci. **13**, 261 (1963).

[12] J. B. Cumming, in *Applications of Computers to Nuclear and Radiochemistry*, edited by G. D. O'Kelley (Office of Technical Services, Washington, D. C., 1963) NAS-NS 3107.

[13] F. Ajzenberg-Selove and T. Lauritsen, in *Landolt-Börnstein Tables*, edited by K. H. Hellwege (Springer-Verlag, Berlin, 1961), New Series, Group 1: Nuclear Physics and Technology, Vol. I.

[14] The use of the literature half-lives instead of our best values would increase only the C^{16} cross sections from targets heavier than Cu by about 4%. The effects for U would be larger but would be within the errors discussed below.

TABLE III. Cross sections for the production of Li^9, C^{16}, and N^{17} from various targets for 1.0- and 2.8-GeV incident protons (mb).

Targets	Li^9 (1)	Li^9 (2.8)	C^{16} [a] (1)	C^{16} [a] (2.8)	N^{17} (1)	N^{17} (2.8)
B	1.20	1.13				
C	0.216	0.236				
N^{14}		0.28[b]				
N^{15}		0.53[b]				
O^{16}	0.106	0.128				
O^{18}	0.59	0.58	1.12	0.90	30.4	25.1
		0.63[b]				
F	0.23	0.284	0.099	0.071	2.03	1.80
Na	0.185	0.302	0.082	0.101	1.07	1.15
Mg	0.130		0.046		0.58	
Al	0.133	0.238	0.050	0.0654	0.66	0.72
Si	0.077		0.023		0.33	
S	0.054		0.017		0.26	
Ca	0.040	0.126	0.010	0.0253	0.150	0.29
Ti	0.125	0.409	0.0335	0.102	0.307	0.775
Ni		0.249		0.046		0.402
Cu	0.120	0.440	0.0184	0.087	0.149	0.65
Nb		0.814		0.136		0.87
Ag	0.220	1.05	0.028	0.176	0.163	0.99
La	0.65	2.63	0.072	0.500	0.390	2.13
Pr	0.393	2.25	0.069	0.413	0.29	2.07
Nd		2.75		0.484		2.20
Ta	0.59		0.099		0.366	
W	0.82	3.9	0.105	0.89	0.393	3.4
Pb		6.0		1.16		4.2
U	1.7	7.5	0.31	1.8	1.1	6.3

[a] Lower limit assuming 100% delayed neutron branch.
[b] At 2.2 GeV. See Ref. 18.

termined that the precision of a measurement was 3%. However, the accuracy of the cross sections has a contribution of 5% from the uncertainty of the neutron counting efficiency (Fig. 2). Of course, there is also the systematic uncertainty of the monitor cross sections.[11]

Delayed-neutron emitters are well-known products of the neutron-induced fission of uranium, thorium, and plutonium. They occur among the neutron-rich isotopes of bromine and iodine and have half-lives ranging from 0.2 to 56 sec. With the exception of uranium none of our targets yielded these isotopes when bombarded with 1- and 2.8-GeV protons. From this observation we may conclude that neither extensive spallation nor high-deposition-energy fission lead to products with a large neutron excess. This conclusion is in agreement with the results of other work on high-energy fission and spallation reactions.[15,16] Rudstam and co-workers[17] have reported two delayed-neutron activities with half-lives of 8 and 18 sec produced from copper by 170-MeV protons. Under our experimental conditions the upper limits which we can set to the production of a delayed-neutron emitter with a half-life of 18 sec is about 1 μb from silver and heavier targets and about 5 μb for copper and lighter targets. In the case of lead we have observed a slightly higher upper limit for long-lived neutron emitters, which in terms of the 18-sec half-life, amounts to 24 μb. This may represent a very small proportion of the fission-product delayed-neutron emitters, but the activity observed was too low to make possible any quantitative study of half-lives and yields. When a search for very short-lived activities was made an 11.4-msec half-life was observed from light-mass targets. This was assigned to Be^{12} and is described in a separate paper.[18]

The absence of the fission-product delayed-neutron emitters from the products of the high-energy reactions studied by us was a very fortunate circumstance, for it enabled us to measure the yields of Li^9, C^{16}, and N^{17} for all targets (except uranium) with good precision. In the case of uranium, a considerable proportion of the observed activity consisted of fission-product delayed-neutron emitters. This again is in agreement with other work[15,16] which shows that typical low-energy fission products, such as Ba^{140} and Kr^{85} are formed in considerable yields in the bombardment of uranium with GeV-energy protons. We have extended this observation by showing that even products far more neutron rich than Kr^{85} and Ba^{140}—the delayed-neutron emitters—are formed in appreciable yields from uranium by GeV-energy protons.

The complex decay curves observed in the experiments with uranium targets were analyzed[12] in terms of eight half-lives. These were the half-lives of Li^9, C^{16}, and N^{17} and five of the six half-life groups reported for the fission-spectrum neutron fission of U^{235} by Keepin[19] (54.5, 21.8, 6.00, 2.23, 0.496, 0.179 sec). Because of the closeness of the half-life values of Li^9 and the last fission-product delayed-neutron group, only one value (0.176 sec) was used to represent both. In calculating the cross section of Li^9 from uranium we have corrected the computed activity by subtracting an estimated fission-product contribution. This estimate was made on the basis of the fractional-yield distribution of the various neutron groups (see Table IV). The choice of the six half-life groups was rather arbitrary because most of the groups probably contain multiple isotopes with similar half-lives and we do not know what the correct mean half-lives are for the high-energy fission of uranium. (This amounts to uncertainty as to the nature of the fissioning nuclides. We have chosen, somewhat arbitrarily, U^{235} as representing these.) This uncertainty, together with the need to fit a decay curve with eight half-lives, some of which are close together, makes our measurements of the cross sections of Li^9, C^{16}, and N^{17} from uranium much less reliable than for the other targets. Particularly uncertain are our values for 1-GeV proton energy, where the contribution of fission-product delayed-neutrons is predominant. The cross sections for this energy reported in Table III should be regarded as being only within a factor of 2 of the true value. The

[15] G. Friedlander, L. Friedman, B. Gordon, and L. Yaffe, Phys. Rev. **129**, 1809 (1963).
[16] I. Dostrovsky and R. W. Stoenner (private communication).
[17] G. Rudstam, Å. Svanheden, and A. C. Pappas, Nature **188**, 1178 (1960).
[18] A. M. Poskanzer, P. L. Reeder, and I. Dostrovsky, Phys. Rev. **138**, B18 (1965).
[19] G. R. Keepin, Nucleonics **20**, 150 (1962).

TABLE IV. Cross sections for the production of fission-product delayed-neutron-emitting groups from uranium with 1- and 2.8-GeV protons.

Half-life group (sec)	Cross section (mb) 1 GeV	2.8 GeV	Fractional yield 1 GeV	2.8 GeV	U^{235} [a]	U^{238} [a]
55	0.17±0.02	0.20±0.02	0.038±0.007	0.046±0.006	0.038	0.013
22	0.62±0.10	0.60±0.06	0.14 ±0.02	0.14 ±0.02	0.21	0.14
6	0.8 ±0.3	1.1 ±0.5	0.18 ±0.07	0.27 ±0.09	0.19	0.16
2.2	1.8 ±0.2	1.4 ±0.6	0.41 ±0.07	0.33 ±0.13	0.41	0.39
0.5	1.1 ±0.2	1.0 ±0.4	0.23 ±0.05	0.22 ±0.08	0.13	0.22
0.18					0.026	0.075
Total	4.5 ±0.4	4.3 ±0.9				

[a] Fission spectrum neutron fission. See Ref. 19.

cross sections for 2.8-GeV protons are better and are probably good to 25%.

The cross sections for five of the six fission-product delayed-neutron groups are collected in Table IV. The values for the 54.5- and 21.8-sec group are probably the most reliable since the shorter lived light-element neutron emitters do not interfere. The other groups probably are not completely resolved from the 4.16-sec N^{17} and the 0.74-sec C^{16}. At 2.8 GeV, targets of two different thicknesses of uranium (see Table II) were bombarded to determine the effect of secondary particles on the cross sections. For the 55- and 22-sec components a secondary correction of (6±2)% per 100 mg/cm^2 was observed in agreement with previous work.[15] This correction has been applied to all five fission-product groups at both energies.

DISCUSSION

The cross sections for the formation of Li^9, C^{16}, and N^{17} as a function of the mass number of the target nuclei are shown in Fig. 3. The main feature of these plots is the rise in cross section with increase in mass number, except for values of A close to that of the target. In the latter region the cross section drops sharply as the mass difference between target and product increases. Another noticeable feature of Fig. 3 is the scatter of the cross-section values, particularly in the region $A = 14$–64. We shall now discuss these features in turn starting with the left-hand steeply descending branch of the cross section-versus-A plots, commonly referred to as the spallation region.

The reactions which lead to the formation of Li^9 from boron and carbon and of C^{16} and N^{17} from O^{18} and F^{19} targets are of the (p,xp) type. The various reactions of this kind observed in our work are summarized in Table V. It will be seen that the cross section of the (p,xp) reaction drops by an order of magnitude when x increases by one. Thus the cross section for the formation of N^{17} from O^{18} is some 15 times that from F^{19}. Similarly for C^{16} the ratio of the $(p,3p)$ and $(p,4p)$ cross sections is about 13. It should also be noted that the cross sections for the reactions listed in Table V are almost independent of the energy of the bombarding

TABLE V. Some (p,xp) reactions.

Reaction	Target	Product	Cross section (mb) 1-GeV p	2.8-GeV p
$(p,2p)$	O^{18}	N^{17}	30.4	25.1
$(p,3p)$	F^{19}	N^{17}	2.03	1.80
	O^{18}	C^{16}	1.12[a]	0.90[a]
	B^{11}	Li^9	1.49	1.41
$(p,4p)$	F^{19}	C^{16}	0.099[a]	0.071[a]
	C^{12}	Li^9	0.216	0.236

[a] Lower limit, assuming 100% delayed neutron branch.

proton. For all but Li^9 from C^{12} the cross section decreases slightly as the proton energy increases from 1 to 2.8 GeV. These properties of (p,xp) reactions observed in the present work agree well with other observations of similar reactions at high energies.[20–22]

Using the procedure described by Dostrovsky *et al.*,[23] we have calculated that C^{16} and N^{17} are very unlikely to be produced by the evaporation of protons from excited N^{17} and O^{18} nuclei. They represent, therefore, residual nuclei from those prompt cascades in O^{18} and F^{19} targets which deposited only a few MeV excitation energy, and are thus called primary products. It follows that the formation of the very neutron-excess isotopes, N^{17}, C^{16}, and Li^9 by (p,xp) reactions from light targets can be used in studies of direct interactions without the complication of the evaporation process.

The formation of these products from slightly heavier targets, as for example, N^{17} from sodium or aluminum, may involve longer spallation chains arising from both prompt cascades and short evaporation chains. Since the residual products from extensive evaporation chains peak near stability or towards the neutron-deficient side of stability, it is clear that the yield of N^{17}, C^{16}, and Li^9 produced as spallation residues will drop off rapidly with the increase in the mass difference between target

[20] P. L. Reeder, University of California Report UCRL 10531, 1962 (unpublished).
[21] S. Meloni and J. B. Cumming, Phys. Rev. **136**, B1359 (1964).
[22] D. L. Morrison and A. A. Caretto, Jr., Phys. Rev. **127**, 1731 (1962).
[23] I. Dostrovsky, Z. Fraenkel, and G. Friedlander, Phys. Rev. **116**, 683 (1959).

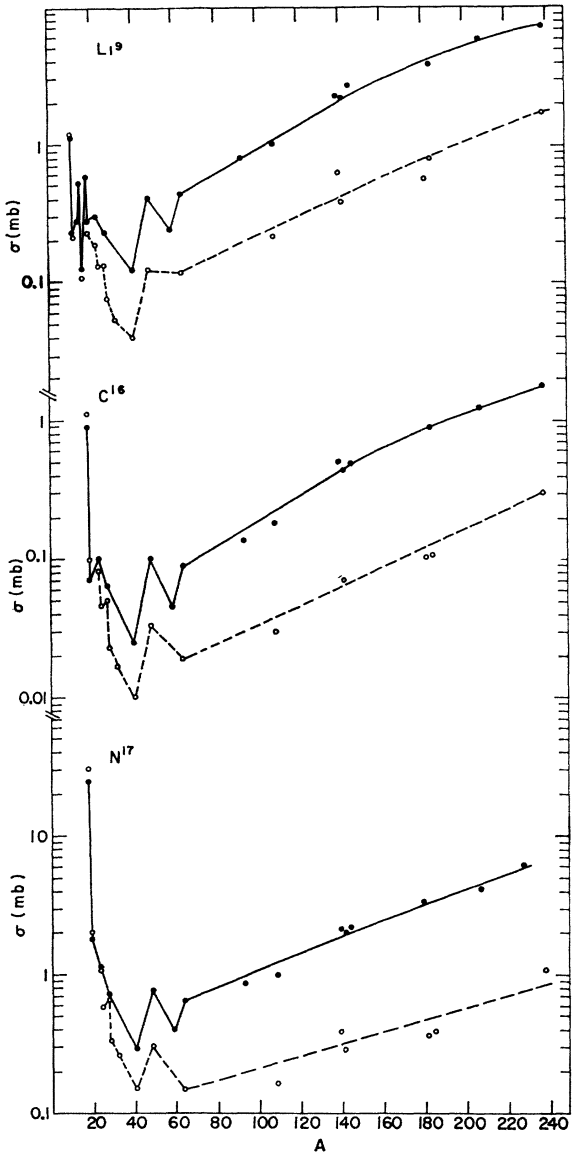

FIG. 3. Cross sections for the production of Li^9, C^{16}, and N^{17} versus target mass number. Solid curves and solid points 2.8 GeV, dashed curves and circles 1 GeV.

and product. Thus the steep left-hand branches of Fig. 3 can be explained in terms of the spallation mechanism.

Products less neutron rich than those discussed above, for example F^{18}, Na^{24}, N^{13}, may be formed as residues from much more extensive spallation processes involving longer evaporation chains. We therefore expect that for such products the left-hand descending branch of the cross section-versus-A plot will be flatter and will extend to higher mass numbers of the target. In Figs. 4(a), 4(b), 4(c) are shown a comparison of the variation of the cross section of a number of light fragments with the mass number of the target. All the neutron excess fragments [Fig. 4(a)] show a steady rise in cross section with A above mass 27. The neutron-deficient products [Fig. 4(c)] on the other hand exhibit a decrease of cross section with A. Products nearer stability [e.g., F^{18} and Na^{24}, Fig. 4(b)] show a two-branched curve with a prominent spallation region at lower target masses.

The apparent scatter of the points in the low-mass region seen in Fig. 3 is not due to experimental errors but rather illustrates the dependence of the cross section on the neutron-to-proton ratio of the target nuclei. In fact, the targets in this region were chosen so

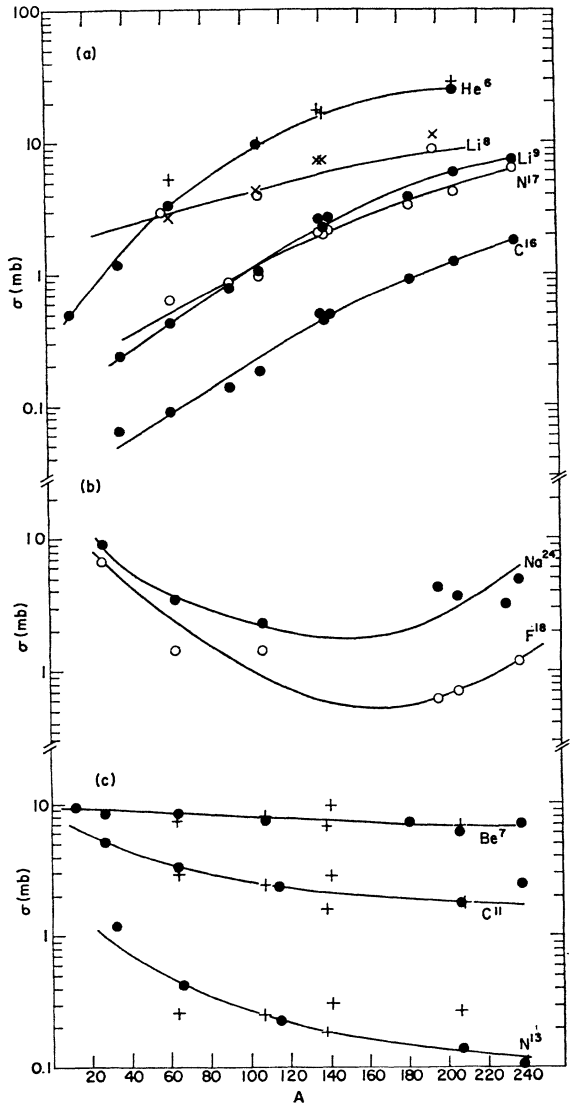

FIG. 4. Comparison of the cross sections of various light fragments at 2.8 GeV. +'s and ×'s are calculated at 1.8 GeV and normalized at $A=108$. (a) Neutron-excess fragments: He^6, see Ref. 1; Li^8, see Refs. 3 and 5 (2.2 GeV). (b) Fragments near the line of beta stability: see Refs. 6 and 7. (c) Neutron-deficient fragments: Be^7, see Refs. 2 and 7; N^{13}, see Refs. 5 and 7; C^{11}, see Refs. 4 and 7.

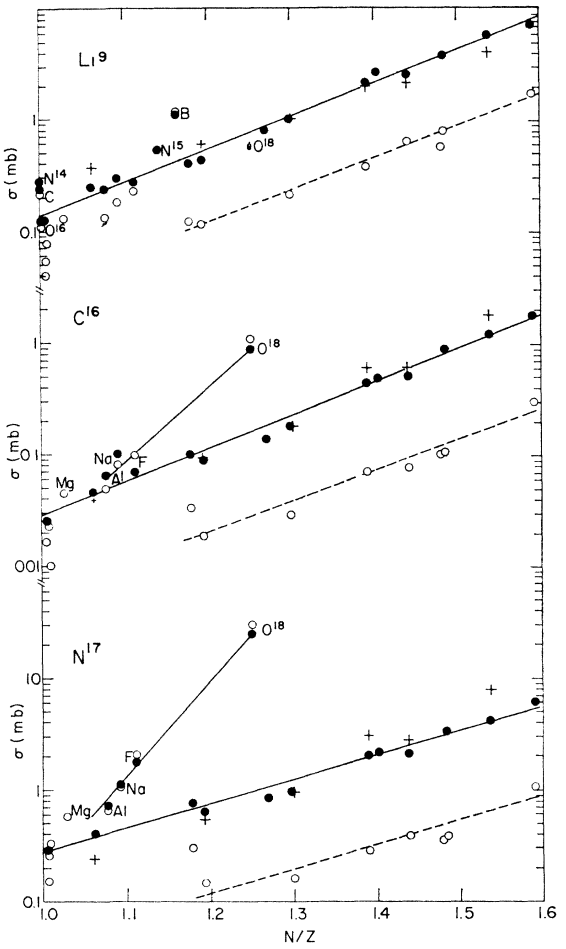

FIG. 5. Cross sections for the production of Li^9, C^{16}, and N^{17} versus neutron-to-proton ratio of the target nucleus. Solid curves and solid points 2.8 GeV, dashed curves and circles 1 GeV. +'s are calculated at 1.8 GeV and normalized at $A=108$.

as to test this point. Pairs of target elements were selected close to each other in mass number but differing as far as possible in their neutron-to-proton ratio. Avoiding the use of separated isotopes the choice is rather limited, and in our case led to the pairs Cu-Ni, Ca-Ti, La-Pr, and Pr-Nd. In addition, we have used two pairs involving a separated isotope, namely O^{16}-O^{18} and N^{14}-N^{15}. As will be noted from Table III, the cross sections for the formation of Li^9, C^{16}, and N^{17} do depend strongly on the neutron-to-proton ratio of the target material. The higher this ratio the greater the cross section. This behavior suggested that if the cross sections were plotted against N/Z of the target material a smoother curve might result. Such plots are shown in Fig. 5. It will be observed that, indeed, a more consistent representation is obtained than in Fig. 3. In these plots again the targets (O^{18}, etc.) from which C^{16} and N^{17} are produced by simple spallation reactions fall on a separate and distinct curve.

The monotonically rising cross sections for Li^9, C^{16}, and N^{17} with N/Z suggest one common mechanism for their formation from targets in the range Al to U. We have seen above that this mechanism cannot be spallation. The fact that the cross sections are still rising considerably with increase in proton energy from 1 to 2.8 GeV also indicates that the mechanism is a high-energy process.

One of the mechanisms proposed for the formation of light fragments in high-energy interactions is fragmentation.[24] This is envisaged as some fast process occurring on a time scale comparable with that of the "prompt" nucleon cascade. No quantitative treatment of such a mechanism exists which will permit the calculation of the dependence of cross section on the mass of the target, on its neutron-to-proton ratio, and on the bombarding energy. We cannot therefore subject fragmentation to a direct test by comparing its predictions with our results. We can, however, investigate whether our results are consistent with other possible mechanisms which are amenable to calculation. A mechanism which has not been considered seriously so far for the formation of light fragments is the well-known evaporation process. Nuclear evaporation has been treated theoretically and its predictions have been extensively tested.[23] It has been shown to account reasonably well for the emission of nucleons and small light fragments from excited nuclei. Some comparisons with experiments have also been made for the evaporation of He^6, Li^8, Be^7, and N^{13} and again a measure of agreement was obtained.[5,25] Our present experiments provide an extensive set of cross sections for a large variety of targets and a more rigorous comparison can therefore be made.

Although the applicability of the statistical model at very high excitation energies is doubtful, we nevertheless decided to explore the predictions of the evaporation theory for the emission of light fragments. We calculated the formation cross sections of Li^9, C^{16}, and N^{17} (and also He^6, Be^7, C^{11}, N^{13}, Ne^{17}, F^{18}, and Na^{24}) as evaporated particles by the Monte Carlo technique[5,25] with the modifications described in the Appendix to this paper.

Absolute cross sections for the evaporation of particles heavier than alpha can only be calculated if proper account is taken of the energies and spins of all relevant states of the particle and its possible progenitors (see Appendix). For the particles of interest in the present work such information is not available. We cannot therefore make any comparisons of the magnitude of the experimental and calculated cross sections. We can, however, make perfectly valid comparisons of the variations of cross section of a given product as a function of target-nuclei mass and composition. These are the main comparisons made in this paper.

The input data for our calculations were the A,Z,E

[24] R. Wolfgang, E. W. Baker, A. A. Caretto, J. B. Cumming, G. Friedlander, and J. Hudis, Phys. Rev. **103**, 394 (1956).
[25] I. Dostrovsky, Z. Fraenkel, and P. Rabinowitz, Phys. Rev. **118**, 791 (1960).

distribution of prompt cascade products computed by Metropolis and co-workers[26] for Cu, Ru^{100}, Ce^{140}, and Bi^{209} at 0.94- and 1.84-GeV proton energy. From these we obtained the distribution for Ni, Ag, La, Pr, and Pb by the shifting procedure described previously.[25] No attempt at parameter fitting was made since the purpose of the calculation was only to check whether evaporation theory is consistent with our observation and not to try to obtain absolute values of cross sections. We have used the value of $a=A/10$ MeV^{-1} for the level-density parameter and $r_0=1.5$ F for the radius parameter.

In comparing calculated and observed cross sections of light fragments it is necessary to consider two further sources of an observed nuclide. We have to allow for a β-chain decay to the nuclide under consideration and also the possibility that neighboring heavier nuclides may be formed with sufficient excitation energy to evaporate one or more particles, i.e., by secondary evaporation. The cross sections for all nuclides calculated in this study, with the exception of F^{18}, Na^{24}, and possibly Li^8, N^{12}, and N^{17} represent independent yields not complicated by β decay because their parents are particle unstable.[27]

As pointed out to us by T. D. Thomas, secondary evaporation can contribute an important fraction of the yield of some nuclides (see Appendix) and has to be taken into account in the calculations of cross sections. For the comparisons made in this paper secondary evaporation is less important since it can be shown that only close neighbors contribute appreciably to the yield. These progenitors are likely to follow a behavior parallel to that of the final product with respect to their dependence of cross section on target mass and composition. The contribution of secondary evaporation was included in the calculations presented in this paper according to the procedure described in the Appendix. Our results and conclusions are, however, quite insensitive to this effect.

The calculated cross sections are compared with the experimental results from our own work in Fig. 5 and with other work in Fig. 4. For the purpose of these comparisons the calculated cross sections at 1.84 GeV were normalized to the experimental value for silver targets at 2.8 GeV. It will be seen that the calculations reproduce the experimental trends of the cross sections with mass and composition fairly well. As a further illustration we have collected in Table VI a few calculated and experimental ratios of the yields from copper and nickel. Again we note that the agreement is reasonably good. The measurement of some of the other ratios included in Table VI for which no experimental values are available at present should provide a further test of the applicability of the evaporation formalism to the emission of light fragments.

TABLE VI. Ratio of yields from Cu to those from Ni for various light fragments.

	Ratio	
	Calculated (1.84 GeV)	Experiment (2.8 GeV)
He^6	1.42	
Li^6	0.85	
Li^7	1.06	
Be^{7} [a]	0.58	
Li^8	1.32	
B^8	0.43	
Li^9	1.66	1.77
C^{11} [a]	0.49	
N^{13} [a]	0.50	
C^{14}	1.10	
C^{16} [a]	2.43	1.98
N^{17} [a]	2.25	1.62

[a] Yield from secondary evaporation included.

The data presented in this paper show that both experimental and calculated cross sections show a strong dependence on the neutron-to-proton ratio of the target material. In the calculated results this dependence arises primarily from differences in the binding energies of the fragments in the evaporating nuclei. We can generalize the predictions of the evaporation theory for the magnitude and direction of the effect of changing N/Z of the target nucleus in different regions of the chart of the nuclides on the cross section of various fragments. If the neutron-to-proton ratio of the fragment is close to the local N/Z ratio of the stability valley in the target region, the evaporating and residual nuclei will be equidistant from the line of beta stability, and no great effect will be observed on the cross section when the target nucleus is varied while keeping A approximately constant. If, on the other hand, the neutron-to-proton ratio of the fragment is very different from that of the beta stability valley, marked changes in the cross section of the reactions will result from small changes of N/Z of the target and therefore a strong target-isotope effect will be observed. For example, evaporation calculations predict that relatively small N/Z effects will be observed for the emission of neutron-excess products from lead isotopes (see N^{17} in Table X, Appendix). The same fragment, however, will show marked increase in cross section with increasing N/Z from targets in the Ni region. Conversely, a fragment with an N/Z ratio close to unity (see F^{18} in Table X, Appendix) will show only a small N/Z effect from targets in the Ni region but an appreciable decrease with increasing N/Z in the lead region. The increase in cross section with N/Z observed for He^6, Li^9, C^{16}, N^{17} and the falling cross sections of C^{11} and N^{13} (see Figs. 4 and 5) can be interpreted as manifestations of the effects summarized above.

The fact that the experimental results for the cross sections of the light-fragment emission exhibit the characteristics predicted by the evaporation theory both

[26] N. Metropolis, R. Bivins, M. Storm, J. M. Miller, G. Friedlander, and A. Turkevich, Phys. Rev. **110**, 204 (1958).

[27] A. I. Baz', V. I. Gol'danskii, and Ya. B. Zel'dovich, Usp. Fiz. Nauk **72**, 211 (1960) [English transl.: Soviet Phys.—Usp. **3**, 729 (1961)].

with regard to general trends and also with regard to specific effects (such as Cu/Ni ratios) is of course very suggestive that the process responsible is indeed one of evaporation. It does not exclude the possibility that a different mechanism is operating which leads to similar predictions for these effects.

One difficulty in accepting the evaporation mechanism in high-energy nuclear reactions derives from the short-time scale of the process at high excitation energies. It is a basic assumption of the statistical model that the lifetime of the excited nucleus not be shorter than its relaxation time. Using Ericson's[28] equation we estimate that for a mass-200 nucleus with an excitation energy of 500 MeV the lifetime for neutron emission is 10^{-22} sec. This is shorter than his estimates of the relaxation time and of the rotation time of the nucleus. In view of this it is surprising that the evaporation formalism which is based on the statistical model has any success in describing the experimental results. This may be either because the relaxation time is in reality much shorter than has been estimated, or the evaporation formalism for calculating cross sections holds approximately even from incompletely equilibrated systems. Ericson[28] indeed suggests that the success of previous calculations of this type does not indicate the existence of a long-lived equilibrium system as an intermediate state, but may rather be regarded as a pure phase-space effect. Thus, he continues, we may have "the usefulness of the statistical model regarded only as a phase-space description. It may then have an approximative validity outside its ordinary range of applicability." In the present case we are considering relative cross sections which are determined by the *ratios* of phase spaces (level densities). It may be that these ratios, although not for long-lived equilibrium systems, reflect aspects of the statistical model such as the mass-energy surface.

Let us now consider the more detailed experiment which has been previously reported concerning differential-range and angular-distribution measurements on the production of Na^{24} from bismuth.[29] This experiment could not be explained by a two-step mechanism in which the second step had no memory of the first, and indicated that the process was faster than the rotation time of the nucleus. This is not inconsistent with the short evaporation time estimated above. Thus the two sets of experiments are not contradictory concerning the time scale. However, it is apparent that neither the Na^{24} energy spectra[29] nor Li^{8} energy spectra[30] can be reproduced correctly by an evaporation calculation with the parameters used in this paper. Thus again we encounter the problem that both cross sections and energy spectra cannot be calculated with the same set of parameters.[31]

A possible process which we have considered briefly dose show some of the qualitative features of the N/Z dependence of the cross sections. According to this mechanism a "cold" fragment is splintered off the nucleus as a consequence of the nucleonic cascade. Qualitatively it will be seen that the composition of such a fragment will reflect that of the target nucleus, and therefore a neutron-rich nucleus will favor the production of neutron-excess fragments over that of neutron-deficient ones. A simple probability calculation, using the Bernoulli theorem, shows, however, that this effect is not large enough to explain the observed variation of the yield with N/Z. Also this mechanism does not provide a clear way of predicting the relative magnitude of the cross sestions.

FISSION PRODUCTS

In Table IV are collected the cross sections for the formation of fission-product delayed-neutron-emitting groups measured from uranium at 1- and 2.8-GeV proton energy. Also included are fractional yields of the various neutron groups and a comparison with U^{235} and U^{238}. It will be noted that the cross sections for these products are energy independent in the range 1–3 GeV. The fractional yields of the various groups are also energy independent and are similar to those observed for the fission-spectrum neutron fission of uranium. Both these facts indicate that the process leading to the formation of the fission-product delayed-neutron emitters in the high-energy bombardment of uranium involves low-energy deposition in the fissioning nuclides. It is interesting in this connection to estimate the proportion of these low-deposition-energy events in uranium. The total cross section for the formation of fission-product delayed-neutron emitters is 4.4 mb. Assuming the value of 0.016 delayed neutron per low-energy fission[19] of U^{236} we can calculate that the low-energy fission cross section is $4.4/0.016 = 280$ mb. This value agrees with the estimate of 330 mb of Friedlander and co-workers[15,32] for the yield of low-deposition-energy events in uranium.

CONCLUSIONS

The variation of the cross sections for the formation of Li^{9}, C^{16}, and N^{17} and other light fragments with target mass and composition suggests that the production process involves the binding energies of the fragments to the parent nucleus and is therefore sensitive

[28] T. Ericson, Advan. Phys. Suppl. **9**, 425 (1960).

[29] J. B. Cumming, R. J. Cross, Jr., J. Hudis, and A. M. Poskanzer, Phys. Rev. **134**, B167 (1964).

[30] N. A. Perfilov, O. V. Lozhkin, and V. P. Shamov, Usp. Fiz. Nauk **60**, 3 (1960) [English transl.: Soviet Phys.—Usp. **3**, 1 (1960)].

[31] I. Dostrovsky, Z. Fraenkel, and L. Winsberg, Phys. Rev. **118**, 781 (1960).

[32] G. Friedlander, in Proceedings of the IAEA Conference on Physics and Chemistry of Fission, Salzburg, 1965, paper SM 60/63 (unpublished). The estimate of 330 mb may be obtained from the value of 13.5 mb for the neutron-excess mass-131 yield at 3 GeV and the 131-mass yield of 4.1% for 50-MeV proton fission.

to the details of the mass-energy surface. The evaporation formalism includes the mass-energy surface in a natural manner. However, the Na^{24} from Bi experiment[29] indicates that the time scale of the process is fast. We conclude that the agreement between the experimental cross sections and the predicted relative yields strongly indicates that some aspect of the evaporation formalism (namely, the mass-energy surface) is an important part of the description of the fast process responsible for the formation of light fragments.

ACKNOWLEDGMENTS

We wish to thank T. D. Thomas, Z. Fraenkel, L. Remsberg, and M. Perlman for many valuable discussions. The able assistance of John Galvin is appreciated. We are grateful to the operating staff of the Cosmotron for their cooperation and assistance during these experiments. The Weizmann Institute of Science is to be thanked for lending us the O^{18} target material.

APPENDIX

In the calculation of the evaporation of heavy fragments it is necessary to consider not only the direct production of each fragment in all its bound states but also the possibility of its formation from a heavier progenitor emitted with sufficient excitation energy to evaporate one or more nucleons and alpha particles. This additional process for the production of light fragments we call secondary evaporation.

In order to estimate the importance of secondary particle evaporation a more detailed calculation of its possible contribution to the yield of several light fragments was carried out.

Preliminary evaporation calculations permitted the selection of all the important progenitors for each of the light fragments of interest (Be^7, C^{11}, N^{13}, C^{16}, N^{17}, F^{18}, Na^{24}). At the same time the appropriate range of excitation energy for each of the progenitors was determined. This was divided into 5-MeV energy bands and the number of levels in each calculated by integrating the level-density formula:

$$\rho = C \exp[2(aE)^{1/2}],$$

where $C=0.25$, $a=A/30$, and E is the excitation energy corrected to the characteristic level in all but odd-odd nuclei.[23] For each energy band, a weighted average excitation energy was chosen in such a way that the number of levels above and below it were the same. For the purpose of the evaporation calculation each energy band of a possible progenitor was considered as a distinct particle with mass equal to the ground-state mass plus the weighted average-excitation-energy and of statistical weight equal to the total number of levels in the band multiplied by four (assuming arbitrarily an average spin of $\frac{3}{2}$). A similar procedure was also used to represent the mass and statistical weight of the particle-stable region (except for Be^7 and N^{13}). This procedure is only suitable for the calculation of the relative contribution of the various progenitors but, of course, leaves the absolute scale of the cross sections quite arbitrary.

In Table VII we show the calculated contribution of various progenitors to the yield of some typical evaporated light fragments from silver and 1.84-GeV protons. It will be noted that in some cases (e.g., N^{13}) secondary evaporation may indeed contribute the major proportion of the yield. We also note that the most important progenitors are those which emit a nucleon or an alpha particle. In Table VIII we show a comparison of the cross sections for Be^7, C^{11}, N^{13}, C^{16}, N^{17}, F^{18}, and Na^{24} calculated with and without taking secondary evaporation into account. The entry for each product nuclide is the ratio of total cross section (including contribution from all progenitors) to that calculated for the direct evaporation of the particular product. The magnitude of these numbers show the importance of secondary evaporation for the various products and targets. The variation of the ratios across a row illustrates the effect of the target on the magnitude of the contribution by progenitors. We note that this effect is relatively small and therefore our comparisons cannot be too sensitive to the precise way in which the contribution of progenitors have been taken into account. This is fortunate

TABLE VII. The calculated contribution (in %[a]) by secondary evaporation of various progenitors to the yield of light fragments from silver at 1.84-GeV proton energy.

	Secondary evaporated particles											
Product	None		p		n		$2n$		np		α		2α	
Be^7	Be^7	77.3	B^8	2.9	Be^8	6.5					C^{11}	12.8		
C^{11}	C^{11}	46.1	N^{12}	23.7	C^{12}	18.8					O^{15}	11.2	Ne^{19}	0.2
N^{13}	N^{13}	19.3	O^{14}	18.2	N^{14}	44.6			O^{15}	14.9	F^{19}	2.9		
C^{16}	C^{16}	57.1			C^{17}	7.4					O^{20}	35.4		
N^{17}	N^{17}	37.6	O^{18}	2.0	N^{18}	37.3	N^{19}	8.9			F^{21}	13.6		
F^{18}	F^{18}	68.2	Ne^{19}	3.5	F^{19}	5.4					Na^{22}	22.6		
Na^{24}	Na^{24}	32.9	Mg^{25}	24.3	Na^{25}	38.1					Al^{28}	4.7		

[a] Based only on the progenitors listed in the table. Minor contributions from other progenitors are omitted.

because our procedure for estimating the contribution from various progenitors is very crude.

In Table IX we present the results of our calculation of the evaporation of a number of light fragments from various targets. Thr numbers in the body of Table IX are in millibarns, but because they have not been normalized in any way, they have no good absolute meaning. The values in each row are strictly comparable, but caution must be exercised in comparing numbers in the same vertical column, for they may require different normalization constants. The ratio of the calculated cross sections at 1.8 GeV to those at 0.9 GeV can be compared with experimental ratios at approximately the same energies for the nuclides[1,2,5,6] He^6, Be^7, N^{13}, F^{18}, and Na^{24}. The experimental ratios for 13 cases differ from the calculated ratios by an average of 34%. However, the experimental ratios have errors of at least 30%. Thus the agreement is quite satisfactory for the energy dependence of the cross sections from 1 to 2 GeV.

In Table X are collected some of the calculated ratios of the cross section of certain light fragments from isotopes of Ni, Ag, and Pb. The experimental measurements of some of these ratios should provide an interesting check on the predictions of the evaporation theory.

TABLE VIII. Ratios of cross sections calculated with the contributions from secondary evaporation to the primary yield. 1.84-GeV incident protons.

Product	Target Ni	Cu	Ag	La	Pb
Be^7	1.20	1.19	1.21	1.14	1.13
C^{11}	2.56	2.44	2.07	1.92	1.80
N^{13}	5.62	5.79	5.20	5.46	4.53
C^{16}	1.64	1.75	1.76	1.74	1.72
N^{17}	2.08	2.51	2.54	2.87	2.87
F^{18}	1.29	1.34	1.40	1.39	1.39
Na^{24}	2.14	2.52	2.89	3.02	2.63

TABLE IX. Calculated cross sections for the evaporation of various light fragments at 0.94- and 1.84-GeV incident proton energy.

Product \ Target	Ni		Cu		Ag		La	Pr	Pb^{208}	
	0.9 GeV	1.8 GeV	0.9 GeV	1.8 GeV	0.9 GeV	1.8 GeV	1.8 GeV	1.8 GeV	0.9 GeV	1.8 GeV
He^6		4.7	2.8	6.7	6.3	12.5	22.6	21.4	11	37
Li^6		26	9.7	22	13.4	30	33	42	10	39
Li^7		18.7	8.5	20	15.7	32	44	50	17	62
Be^7 [a]	9.7	21	9.3	12	4.1	13	11	16	2.0	10.2
Li^8		4.4	2.0	5.8	4.4	9.4	16.1	16.4	5.5	25
B^8		2.0	0.27	0.85	0.20	0.64	0.33	0.62	0.039	0.23
Li^9		0.35	0.18	0.58	0.47	1.0	2.1	1.95	0.84	3.9
Be^{10}		2.2	1.6	2.7	2.2	4.3	7.6	8.3	3.1	13.0
C^{11} [a]	2.0	4.1	0.59	2.0	0.42	1.7	1.1	2.0	0.18	1.16
N^{13} [a]	0.75	1.2	0.25	0.67	0.17	0.65	0.42	0.82	0.13	0.67
O^{13}		0.042	0.0048	0.012	0.0019	0.0067	0.0021	0.0059	0.00094	0.0019
C^{14}		0.48	0.26	0.53	0.46	0.86	1.6	2.0	0.97	3.6
C^{16} [a]	0.0014	0.0023	0.0028	0.0056	0.0074	0.011	0.036	0.037	0.024	0.11
N^{17} [a]	0.015	0.023	0.026	0.052	0.051	0.093	0.26	0.29	0.14	0.73
Ne^{17}		0.011	0.0017	0.0029	0.00048	0.0018	0.00047	0.0016	0.00007	0.00060
F^{18} [a]					0.054	0.21	0.18	0.33	0.12	0.46
Na^{24} [a]					0.023	0.063	0.11	0.17	0.14	0.52

[a] Secondary evaporation included.

TABLE X. Calculated cross-section ratios for the evaporation of selected light fragments from separated isotope targets (1.84-GeV protons).

	Ni^{60}/Ni^{58}	Ag^{109}/Ag^{107} [a]	Pb^{208}/Pb^{206}
Li^6 [b]	0.90		0.87
Li^7 [b]	1.06		0.92
Be^7	0.74	0.80	0.80
C^{11}	0.68	0.78	0.75
C^{14} [b]	1.17	...	0.88
N^{13}	0.73	0.89	0.84
N^{17}	1.83	1.51	0.94
Ne^{17} [b]	0.42	0.43	0.60
F^{18}	0.89	0.83	0.75

[a] 0.94-GeV incident protons.
[b] Secondary evaporation not included.